Journal of Alloys and Compounds 488 (2009) 232–237

Contents lists available at ScienceDirect

Journal of Alloys and Compounds

journal homepage: www.elsevier.com/locate/jallcom

Microstructure and optical properties of polycrystalline ZnO films sputtered under different oxygen flow rates

X.C. Wang*, X.M. Chen, B.H. Yang

Tianjin Key Laboratory of Film Electronic & communicate Devices, School of Electronics Information Engineering, Tianjin University of Technology, Tianjin 300191, People's Republic of China

ARTICLE INFO

Article history:
Received 2 July 2009
Received in revised form 19 August 2009
Accepted 20 August 2009
Available online 27 August 2009

PACS:
68.55.−a
68.55.Ln
78.20.−e
78.55.−m

Keywords:
Thin films
Semiconductors
Optical properties
Crystal structure and symmetry

ABSTRACT

Polycrystalline ZnO films were fabricated using rf magnetron sputtering under different oxygen flow rates (P_O). The surface morphology of the films can be affected by changing P_O, and the average surface roughness decreases with the increasing P_O. The increasing P_O can improve the grain growth with (0 0 2) orientation. Typical ZnO infrared vibration bands have been observed at 408 and 513 cm^{-1}, and the full width at half maximum of the infrared peak decreases with the increase of P_O due to the improved crystallinity. The optical band gap (E_g) of the polycrystalline ZnO films increases from 3.22 eV at P_O = 0 sccm to 3.25 eV at P_O = 10 sccm because the defects decrease with the increasing P_O. The photoluminescence peaks in the region of 2.4–2.7 eV are from the transition between conduction band edge and oxide antisite defects (O_{Zn}), and also be influenced by oxygen vacancies (V_O).

© 2009 Elsevier B.V. All rights reserved.

1. Introduction

ZnO with wide band gap (3.37 eV) and large binding energy (60 meV) has attracted considerable attention from both fundamental and application points of view, such as solar cells, blue and ultraviolet light emitting devices [1–4]. Furthermore, ZnO nanostructures can also be used in various applications such as nanowire, nanolasers, biosensors and field emission devices [5]. Piezoelectric properties of ZnO are being explored for fabrication of various pressure transducers, acoustic and optoacoustic devices [6]. Zn vacancies induced magnetic order in the pure ZnO films has been reported by Khalid et al. [7]. With the development of material science, ZnO will offer more applications in the associated fields. Nano-size polycrystalline and epitaxial ZnO films have been extensively fabricated by using several methods including pulse laser deposition [8,9], molecular beam epitaxy [10–12], magnetron sputtering [13,14], oxidation of metallic zinc films [15], sol–gel method [16], etc. The surface morphology, microstructure, film growth, electrical and optical properties of ZnO films can be affected by the experimental conditions, such as substrates, fabrication methods, oxygen flow rate, and element doping [17–21], which can be ascribed to the change of the defects in the films. It is well known that the sputtering technology is an effective and the most widespread method for fabricating thin films in industry nowadays, and the oxygen flow rate can affect the intrinsic defects in the ZnO films during the film deposition significantly. In this paper, polycrystalline ZnO films were fabricated using rf magnetron sputtering from ZnO target under different oxygen flow rates. Morphology, microstructure and optical properties of the polycrystalline ZnO films are investigated systematically using atomic force microscopy, X-ray diffraction, infrared spectroscopy, UV–vis transmission spectroscopy, and photoluminescence spectroscopy.

2. Experimental details

Polycrystalline ZnO films were fabricated using rf magnetron sputtering method at room temperature from ZnO target in Ar and O_2 gas mixture on glass and Si (1 0 0) wafers with natural oxide layer. The base pressure of the chamber reached 6.0×10^{-6} Pa or better. During the film deposition, the total pressure of sputtering gas was kept at 1.0 Pa (100 sccm) and the O_2 flow rate (P_O) was changed from 0 to 10 sccm. The film thickness was about 300 nm determined using a Dektak 6 M surface profiler. The morphology, structure, and chemical states of the films were characterized using atomic force microscopy (AFM), X-ray diffraction (XRD), and Fourier transform infrared spectroscopy (FTIR, Brucker 8 V). The UV–vis transmission spectra were measured using the UVPC spectrophotometer system (Shimadz

* Corresponding author. Tel.: +86 22 23679372; fax: +86 22 23679457.
E-mail address: wangxccn@126.com (X.C. Wang).

0925-8388/$ – see front matter © 2009 Elsevier B.V. All rights reserved.
doi:10.1016/j.jallcom.2009.08.089

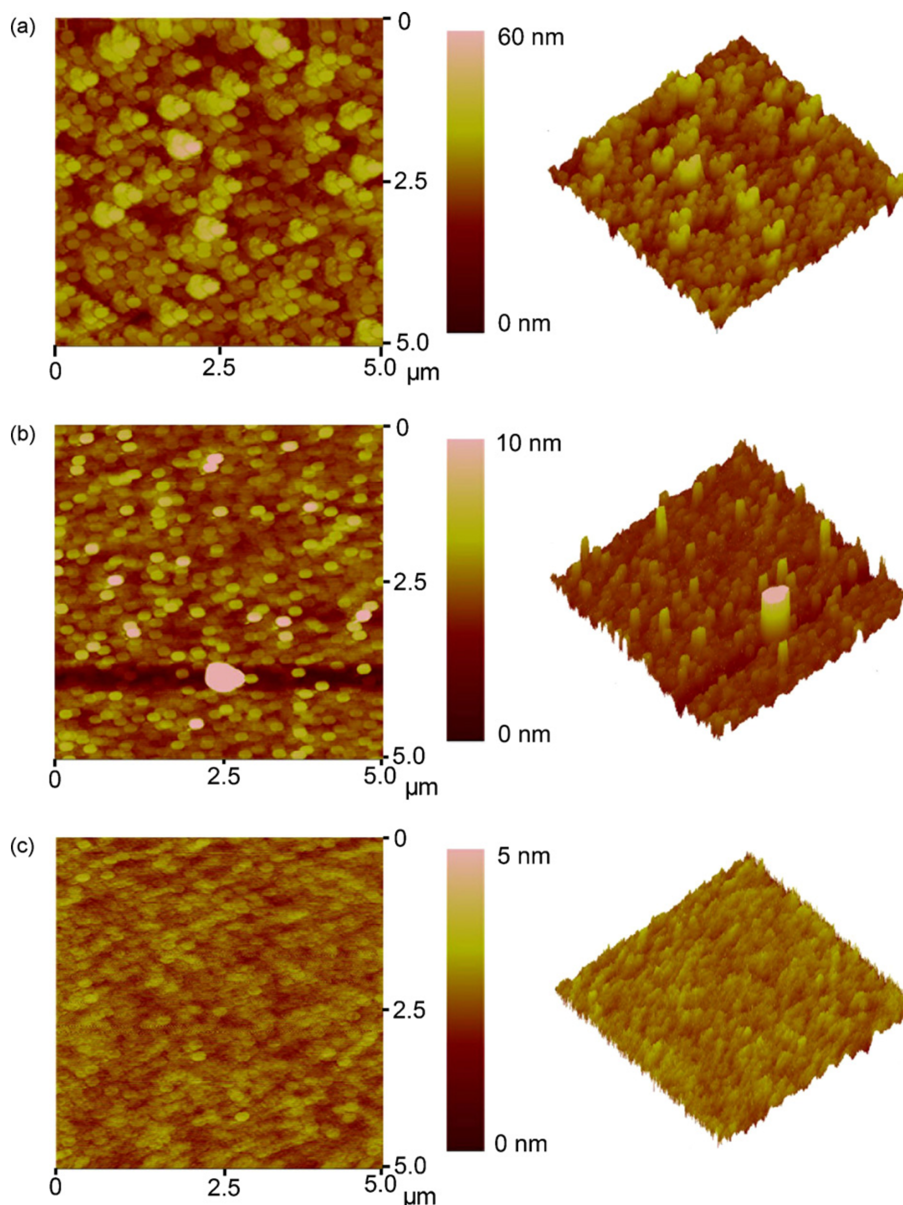

Fig. 1. AFM images of the polycrystalline ZnO films fabricated at different P_O, (a) P_O = 0 sccm, (b) P_O = 2 sccm, and (c) P_O = 6 sccm.

3101 PC). Photoluminescence spectra (PL) were used to study luminescence properties of the films recorded by a Hitachi F-4500 fluorescence spectrophotometer with Xenon lamp as the excitation light source at room temperature.

3. Results and discussion

3.1. Morphology and microstructure

Fig. 1 shows the AFM images of the polycrystalline ZnO films fabricated at different P_O. From this figure, one can see that at P_O = 0 sccm, the film surface is composed of uniform clusters with a size of 500 nm, and the clusters are composed of several uniform 200-nm islands. For observing the surface morphology of the film clearly, the large-scale AFM image of the film fabricated at P_O = 0 sccm is given in Fig. 2. From Fig. 2, one can see that the islands on the film surface are so uniform, and the distance between the large clusters is similar, but the film surface is not so smooth. At P_O = 2 sccm, there are some rods with the diameter of about 200 nm on the film surface, and the rods are separated with the large distance of 300–2000 nm and arbitrary distribution. The film surface looks more smooth, and the longitudinal height is in the scale of 10 nm. As P_O increases to 6 sccm, no obvious islands can be observed on the film surface, and the film surface is so smooth in the scale of 5 nm. The average surface roughness R_a is defined as the arithmetic average deviation from the mean line within the assessment length L

$$R_a = \frac{1}{L}\int_{x=0}^{x=L} |y|dx, \quad (1)$$

where x is the displacement along the lateral scan direction and y is the vertical fluctuation. The average surface roughness of the films decreases from 5.155 nm at P_O = 0 sccm to 0.419 nm at P_O = 6 sccm. The surface morphology should be determined by crystal growth mechanisms and the diffusion behavior during the film deposition. In the present samples, the change of the oxygen flow rate can affect the crystal growth and diffusion of the atoms/ions deposited on the substrates, so the surface morphology of the films fabricated at different P_O is different.

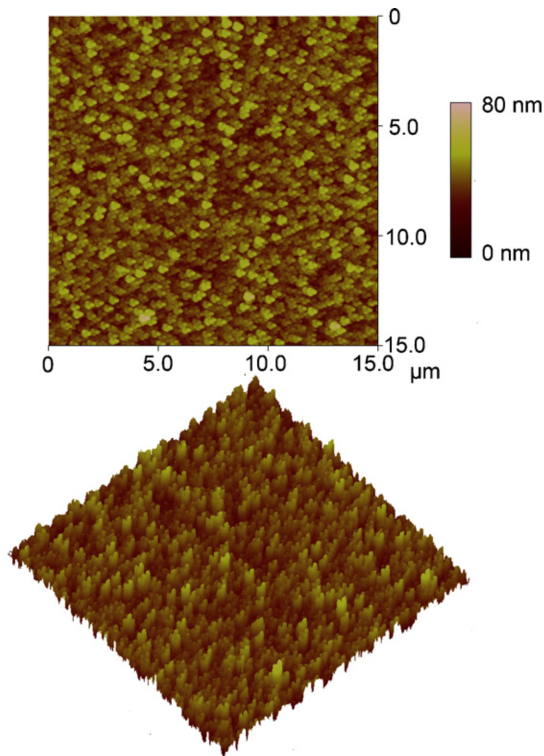

Fig. 2. Large scale AFM images of the polycrystalline ZnO films fabricated at P_O = 0 sccm.

For investigating the crystallization and the growth orientation of the ZnO grains in the films, Fig. 3 presents the XRD patterns of the polycrystalline ZnO films fabricated at different P_O. The wide signal presented between 20° and 40° is from the glass substrates. From Fig. 3(a), the strongest peak situates at 34.5° corresponding to wurtize ZnO (0 0 2), and the intensity ratio of the peaks from different orientations is not the same as that of ZnO powders without a certain orientation. The other diffraction peaks are from ZnO (1 0 1), (1 0 2), (1 0 3), (2 0 1) and (0 0 4). However, the intensity of (1 0 1) and (1 0 3) peaks is larger than that of (0 0 4) peak. So the ZnO film fabricated at P_O = 0 sccm does not grow with (0 0 2) orientation, and the orientation of the ZnO grains in the film is random. At P_O = 1 sccm, there are only two obvious diffraction peaks from (0 0 2) and (0 0 4) planes. The shoulder at 36.4° and a small peak at 62.7° are from (1 0 1) and (1 0 3) planes, as shown in Fig. 3(b). With the further increase of P_O, the shoulder at 36.4° and the peak at 62.7° disappear gradually, and only the peaks from ZnO (0 0 2) and (0 0 4) can be observed in Fig. 3(c)–(g), suggesting that the films fabricated at higher P_O grow with (0 0 2) orientation. The enhanced (0 0 2) orientation growth by increasing P_O was also observed in the ZnO films fabricated by sputtering Zn target in the Ar and O_2 gas mixture [22], so the (0 0 2) orientation growth by increasing the P_O can be ascribed to the decrease of oxygen vacancies. It is well known that the full width at half maximum (FWHM) of the diffraction peaks can be affected by the grain size and strain. In Fig. 3, with the increase of P_O, the FWHM of the diffraction peaks decreases, showing the increased ZnO grain size and/or weakened strain in the films with the increasing P_O.

Wurtzite ZnO belongs to the space group C_{6v}^4 with two formula units in the primitive cell. The optical phonons at the Γ point of the Brillouin zone have the following irreducible representation [23,24]

$$\Gamma_{\rm opt} = 1A_1 + 2B_1 + 1E_1 + 2E_2, \quad (2)$$

where A_1 and E_1 modes are polar and split into transverse (TO) and longitudinal optical (LO) phonons, and they are both infrared and Raman active [25]. The nonpolar E_2 modes are Raman active only. For investigating the Zn–O bonds, the FTIR spectra of the polycrystalline ZnO films fabricated at different P_O are shown in Fig. 4. Theoretical calculation results show a strong IR band at 406 cm^{-1} and one of small intensity at 580 cm^{-1} for slab-type ZnO particles ($c/a \ll 1$) [26]. Hayashi et al. analyzed the surface phonon modes of ZnO small crystals using the FTIR spectra [27]. The FTIR spectra of the ZnO films on Si substrates show a strong peak at 408 cm^{-1} and two weak peaks at 513 and 567 cm^{-1} [28]. In the present FTIR spectra, the peaks are mainly situated at 276, 408, 513 and 595 cm^{-1}. The peaks located at 408 and 513 cm^{-1} are from Zn–O bonds, which is consistent with the previous report [28]. The other two peaks observed at 276 and 595 cm^{-1} are the results of the host lattice defects. In addition, at P_O = 0 sccm, the peak near 408 cm^{-1} shifts to 418 cm^{-1}, and there appears such a weak peak at 380 cm^{-1} because the optical modes of the Zn–O bonds can be decided by the bond length, bond angle, bond strength, and atomic coordination numbers [29]. There are defects in the films fabricated at P_O = 0 sccm so that the bond length, bond angle and bond strength of the Zn–O bonds can be affected. When the bond strength is enhanced, the peak shifts to 410 cm^{-1}, and the peak is at 380 cm^{-1} as the bond strength is weakened. The FWHM of the peak situated at 408 cm^{-1} decreases with the increase of P_O but no significant change in the peak position is observed. The FWHM values of the peaks at 408 cm^{-1} are given in Table 1. Larger FWHM value indicates wider distribution of vibration energy of the Zn–O bonds [28]. The decreasing FWHM with the increasing P_O shows that the vibration energy becomes narrower, which suggests that the crystallinity of the sputtered ZnO films is improved as P_O increases.

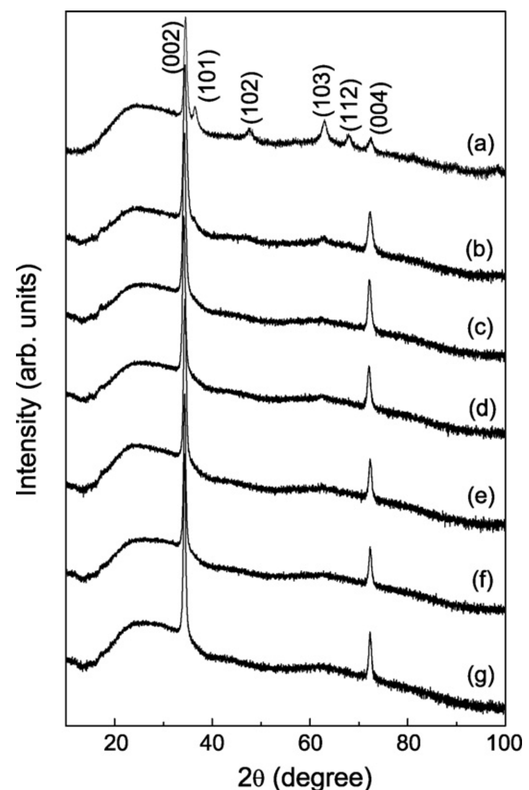

Fig. 3. XRD patterns of the polycrystalline ZnO films fabricated at different P_O, (a) P_O = 0 sccm, (b) P_O = 1 sccm, (c) P_O = 2 sccm, (d) P_O = 4 sccm, (e) P_O = 6 sccm, (f) P_O = 8 sccm, and (g) P_O = 10 sccm.

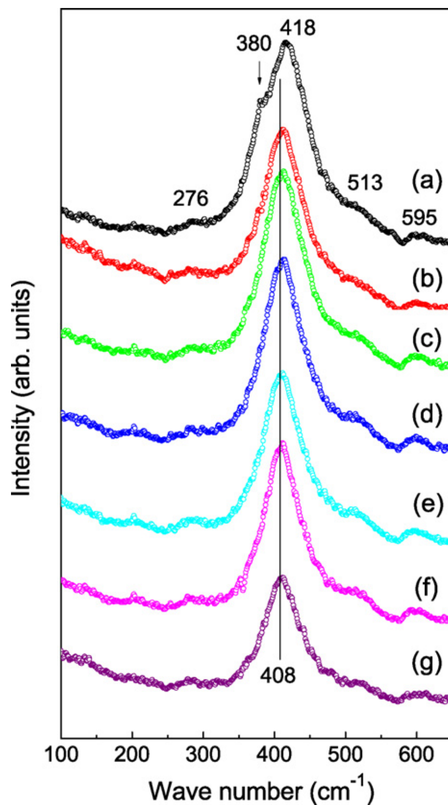

Fig. 4. FTIR spectra of the polycrystalline ZnO films fabricated at different P_O.

3.2. Optical characteristics

Fig. 5 shows transmission spectra of the polycrystalline ZnO films fabricated at different P_O. The spectra of the films show waveforms (ripples), which is the characteristic of the interference of light. The transmission spectra in the visible optical region are transparent, and the transmittance maxima of the polycrystalline ZnO films are near 90%. Due to the fundamental absorption in the vicinity of the band gap, the transmittance decreases sharply as the wavelength reaches the ultraviolet range. It can be found that the absorption edge shifts monotonically to the shorter wavelength as P_O increases, which is correlated to the change in the optical band gap value. It is well known that the absorption edge of the glass substrates are much smaller than that of ZnO, so the absorption edge shown in Fig. 5 is from the ZnO films, but not from glass substrates. The optical band gap E_g can be derived from the absorption coefficient α calculated as a function of incident photon energy $E(h\nu)$. Near the absorption edge, α can be expressed as [30,31]

Table 1
The full width at half maximum (FWHM) of FTIR peak at 408 cm^{-1} from the polycrystalline ZnO films.

P_O (sccm)	0	1	2	4	6	8	10
FWHM (cm^{-1})	83	69	67	64	57	53	50

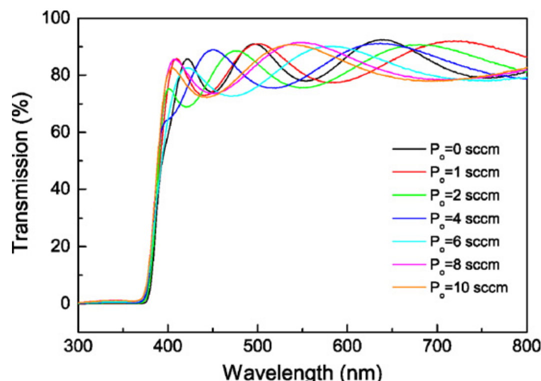

Fig. 5. Transmission spectra of the polycrystalline ZnO films fabricated at different P_O.

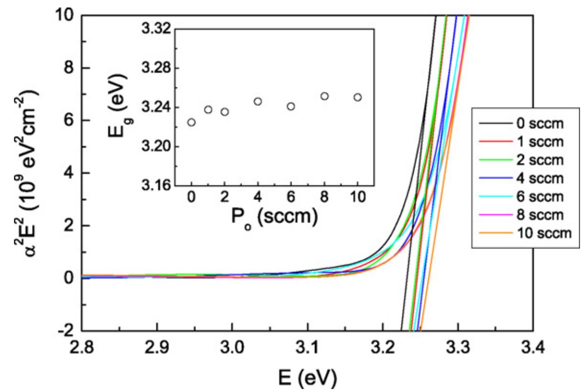

Fig. 6. Dependence of $(\alpha h\nu)^{1/2}$ on photon energy for the polycrystalline ZnO films fabricated at different P_O. The inset gives the derived optical band gap value.

$$\alpha = \frac{-\ln(T)}{d}, \qquad (3)$$

where d is the film thickness. The optical band gap E_g can be derived from the expression of [30,31]

$$\alpha\, h\nu \propto (h\nu - E_g)^m, \qquad (4)$$

where $m = 0.5$ for the direct allowed transition. Fig. 6 presents the dependence of $(\alpha h\nu)^{1/2}$ on photon energy for the polycrystalline ZnO films fabricated at different P_O. The E_g value can be obtained by extrapolating the linear portion to the photon energy axis, as shown in the inset of Fig. 6. There is substantial variation in the values of the optical band gap quoted for ZnO films, and there are three distinct values quoted for ZnO single crystals of 3.1, 3.2 and 3.3 eV. Whilst it can be argued that the higher value must correspond to the true band gap [32]. The variability in the reported values of the band gap in the films can be rationalized on the basis of the presence of growth stresses, thermal expansion mismatch stresses and dopants [30]. The derived optical band gaps of the present films ranging from 3.2 to 3.3 eV are smaller than that of single crystalline ZnO with the band gap of 3.3 eV. Meanwhile, with the increase of P_O, the optical band gap value increases from 3.22 eV at P_O = 0 sccm to 3.25 eV at P_O = 10 sccm. Srincant et al. [30] reports a valence band-donor transition at 3.15 eV, which suggests that the presence of vacancies and dopants decreases the band gap of ZnO films. Therefore, the increase of band gap of the present ZnO films with P_O may be due to the decrease of the defects.

Fig. 7 displays the PL spectra of the polycrystalline ZnO films fabricated at different P_O. Each PL spectrum has been deconvoluted into multipeaks. The fitted peak positions are mainly at 2.46, 2.65, 2.74, 2.81, 2.90, 2.99, 3.09 and 3.20 eV, and smaller than the band gap energy of ZnO film (3.3 eV), which should be related to a local level in band gap due to the presence of defects. At different P_O, the peaks at a certain energy disappear due to the different local level in the band gap as P_O changes. The broad blue emission peak near 2.4–2.7 eV are usually observed, which extends in both directions to green light and near UV band (See Table 2). The blue green light may originate from the electron transition from the bottom of conduction band to oxygen antisite (O_{Zn}) level [33] because the energy gap between the bottom of conduction band to O_{Zn} level is 2.38 eV,

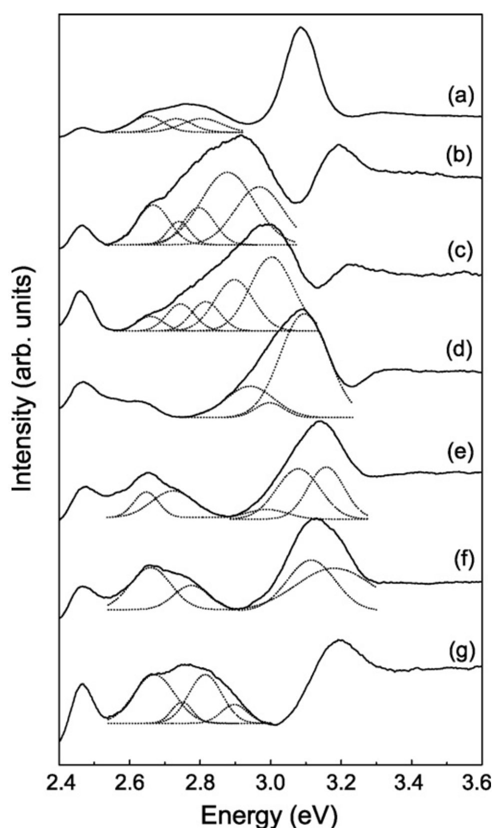

Fig. 7. Photoluminescence spectra of the polycrystalline ZnO films fabricated at different P_O, (a) P_O = 0 sccm, (b) P_O = 1 sccm, (c) P_O = 2 sccm, (d) P_O = 4 sccm, (e) P_O = 6 sccm, (f) P_O = 8 sccm, and (g) P_O = 10 sccm.

which is well consistent with the energy of blue green light but different from the energy interval of other defects. According to the first principle calculation, the oxygen vacancies are easy to form for its low formation energy and the oxygen vacancies combine with the vacancies in the valance band after capturing photo-induced electrons, which gives rise to blue green luminescence [34]. After the oxidation at 600 °C, no deep level or trap state defect emission in the green region can be observed, indicating the absence of interstitial zinc or oxygen vacancies in the films [35]. A blue shift in violet emission with the reduction in crystal size of ZnO nanorods [36]. Especially, the quasi-LO phonon mode is related to the specific defects those strongly affect the optical properties of materials such as ZnO [37]. The greatest Raman shift to lower wave number for the ZnO annealed in ambient atmosphere was observed, which suggests that it has the largest concentration of defects that may be related to the green light emission [37]. The near UV emission peak at 384 nm (3.24 eV) is also observed in the PL spectra of the ZnO films incorporated with low nitrogen contents [38], which corresponds to the band gap of bulk ZnO, which is from the recombination of free excision. All of these suggest that the blue green luminescence has a close relation to the V_O.

All the polycrystalline ZnO films fabricated at different P_O have a high resistivity larger than 10^7 Ω m near our experimental extreme of physical property measurement system so that the Hall effect cannot be measured precisely and the carrier type cannot be determined.

Table 2
The photoluminescence (PL) peak position of the ZnO films fabricated at different O_2 flow rate (P_O).

P_O (sccm)	0	1	2	4	6	8	10
Peak position (eV)	2.47	2.46	2.46	2.47	2.47	2.46	2.47
	2.65	2.67	2.66	2.64	2.65	2.66	2.67
	2.73	2.74	2.75	–	2.73	2.76	2.75
	2.81	2.80	2.81	–	–	–	2.82
	–	2.89	2.89	2.92	–	–	2.90
	–	2.97	3.00	2.99	–	–	–
	3.09	–	–	3.09	3.08	3.12	–
		3.19	3.22	–	3.18	3.19	3.20

4. Conclusions

The morphology, structure and optical properties of the polycrystalline ZnO films fabricated using magnetron sputtering under different P_O have been investigated in details. The surface morphology of the films is affected by P_O. The increase of P_O can improve the growth with (0 0 2) orientation. Typical ZnO infrared bands have been observed at 408 and 513 cm^{-1}. The optical band gap (E_g) of the polycrystalline ZnO films increases from 3.22 to 3.25 eV as P_O increases from 0 to 10 sccm because the defects decrease with the increase of P_O. The blue photoluminescence peaks in the energy range from 2.4 to 2.7 eV come from the transition between conduction band edge and oxide antisite defects, and oxygen vacancies.

Acknowledgements

The work described in this paper is supported by National Science Foundation of China (60576011 and 50701033), the Research Fund for the Doctoral Program of Higher Education (20070056047), Tianjin Natural Science Foundation (08JCYBJC09400 and 06TXTJJC14701).

References

[1] D.C. Kundaliya, Nat. Mater. 3 (2004) 709.
[2] J. Elanchezhiyan, K.P. Bhuvana, N. Gopalakrishnan, T. Balasubramanian, J. Alloys Compd. 463 (2008) 84.
[3] L.H. Van, M.H. Hong, J. Ding, J. Alloys Compd. 449 (2008) 207.
[4] C. Song, K.W. Geng, F. Zeng, X.B. Wang, Y.X. Shen, F. Pan, Y.N. Xie, T. Liu, H.T. Zhou, Z. Fan, Phys. Rev. B 73 (2006) 024405.
[5] S.J. Pearton, D.P. Norton, K. Ip, Y.W. Heo, T. Steiner, J. Vac. Sci. Technol. B 22 (2004) 932.
[6] J. Liu, P. Fei, J.H. Song, X.D. Wang, C.S. Lao, R. Tummala, Z.L. Wang, Nano Lett. 8 (2008) 328.
[7] M. Khalid, M. Ziese, A. Setzer, P. Esquinazi, M. Lorenz, H. Hochmuth, M. Grundmann, D. Spemann, T. Butz, G. Brauer, W. Anwand, G. Fischer, W.A. Adeagbo, W. Hergert, A. Ernst, Phys. Rev. B 80 (2009) 035331.
[8] Y.R. Ryu, S. Zhu, J.D. Budai, H.R. Chandrasekhar, P.F. Miceli, H.W. White, Appl. Phys. Lett. 88 (2000) 201.
[9] H.B. Sang, S.Y. Lee, B.J. Jin, S. Im, Appl. Surf. Sci. 154–155 (2000) 458.
[10] D.C. Look, D.C. Reynolds, C.W. Litton, R.L. Jones, D.B. Eason, G. Cantwell, Appl. Phys. Lett. 81 (2002) 1830.
[11] F.X. Xiu, Z. Yang, L.J. Mandalapu, D.T. Zhao, J.L. Liu, Appl. Phys. Lett. 87 (2005) 252102.
[12] Y.W. Heo, D.P. Norton, S.J. Pearton, J. Appl. Phys. 98 (2005) 073502.
[13] P.F. Carcia, R.S. McLean, M.H. Reilly, G. Nunes, Appl. Phys. Lett. 82 (2003) 1117.
[14] S.H. Jeong, B.S. Kim, B.T. Lee, Appl. Phys. Lett. 82 (2003) 2625.
[15] Y.I. Alivov, A.V. Chernykh, M.V. Chukichev, R.Y. Korotkov, Thin Solid Films 473 (2005) 241.
[16] M.N. Kamalasanan, S. Chandra, Thin Solid Films 288 (1996) 112.
[17] Y. Caglar, S. Ilican, M. Caglar, F. Yakuphanoglu, J.S. Wu, K. Gao, P. Lu, D.F. Xue, J. Alloys Compd. 481 (2009) 885.
[18] X.Y. Zhou, S.H. Ge, D.S. Yao, Y.L. Zuo, Y.H. Xiao, J. Alloys Compd. 463 (2008) L9.
[19] J.H. Yang, X.Y. Liu, L.L. Yang, Y.X. Wang, Y.J. Zhang, J.H. Lang, M. Gao, B. Feng, J. Alloys Compd. 477 (2009) 632.
[20] H.C. Cheng, C.F. Chen, C.Y. Tsay, J.P. Leu, J. Alloys Compd. 475 (2009) L46.
[21] K.J. Chen, F.Y. Hung, S.J. Chang, S.J. Young, J. Alloys Compd. 479 (2009) 674.
[22] R.J. Hong, H.J. Qi, J.B. Huang, H.B. He, Z.X. Fan, J.D. Shao, Thin Solid Films 473 (2005) 58.
[23] N.C. Saha, H.G. Tompkins, J. Appl. Phys. 72 (1992) 3072.
[24] H.M. Zhong, J.B. Wang, X.S. Chen, Z.F. Li, W.L. Xu, W. Lu, J. Appl. Phys. 99 (2006) 103905.
[25] C.A. Arguello, D.L. Rousseau, S.P.S. Porto, Phys. Rev. 181 (1969) 1351.
[26] M. Andres-Verges, A. Mifsud, C.J. Serna, J. Chem. Soc., Faraday Trans. 86 (1990) 959.
[27] S. Hayashi, N. Nakamori, H. Kanamori, Y. Yodogawa, K. Yamamoto, Surf. Sci. 86 (1979) 665.

[28] D.C. Agarwal, R.S. Chauhan, A. Kumar, D. Kabiraj, F. Singh, S.A. Khan, D.K. Avasthi, J.C. Pivin, M. Kumar, J. Ghatak, P.V. Satyam, J. Appl. Phys. 99 (2006) 123105.
[29] M.X. Gu, L.K. Pan, B.K. Tay, C.Q. Sun, J. Raman Spectrosc. 38 (2007) 780.
[30] T. Asanuma, T. Matsutani, C. Liu, T. Mihara, M. Kiuchi, J. Appl. Phys. 95 (2004) 6011.
[31] S.W. Xue, X.T. Zu, W.L. Zhou, H.X. Deng, X. Xiang, L. Zhang, H. Deng, J. Alloys Compd. 448 (2008) 21.
[32] T.C. Damen, S.P.S. Porto, B. Tell, Phys. Rev. 142 (1966) 570.
[33] V. Srinkant, D.R. Clarke, J. Appl. Phys. 83 (1998) 5447, and references therein.
[34] M. Futsuhara, K. Yoshioka, O. Takai, Thin Solid Films 322 (1998) 274.
[35] S.M. Wang, G.D. Xia, J.D. Shao, Z.X. Fan, J. Alloys Compd. 424 (2006) 304.
[36] J.H. Yang, J.H. Lang, L.L. Yang, Y.J. Zhang, D.D. Wang, H.G. Fan, H.L. Liu, Y.X. Wang, M. Gao, J. Alloys Compd. 450 (2008) 521.
[37] Y.Y. Tay, T.T. Tan, M.H. Liang, F. Boey, S. Li, Appl. Phys. Lett. 93 (2008) 111903.
[38] X.C. Wang, W.B. Mi, S. Dong, X.M. Chen, B.H. Yang, J. Alloys Compd. 478 (2009) 507.